Supplementary Information of

# Estimation of FMO3 ontogeny by mechanistic population pharmacokinetic modelling of risdiplam and its impact on drug-drug interactions in children

Clinical Pharmacokinetics

Yumi Cleary[1,2], Heidemarie Kletzl[1], Paul Grimsey[3], Katja Heinig[1], Kayode Ogungbenro[2], Hanna E. Silber Baumann[1], Nicolas Frey[1], Leon Aarons[2], Aleksandra Galetin[2] and Michael Gertz[1]

[1]Roche Pharma Research and Early Development, Roche Innovation Center Basel, Basel, Switzerland; [2]Centre for Applied Pharmacokinetic Research, University of Manchester, Manchester, UK; [3]Roche Pharma Research and Early Development, Roche Innovation Center Welwyn, UK.

Corresponding authors: Yumi Cleary (yumi.cleary@roche.com) and Michael Gertz (michael.gertz@roche.com)

# TABLE OF CONTENTS

## 1. Risdiplam data set used for model development and evaluation/validation

The demographics and plasma concentrations determined in healthy individuals or patients with SMA who participated in the following five clinical studies (**Table S1**) were included in the analyses. Individual plasma concentrations of risdiplam used in the analyses are shown in **Fig. S1**. Data collected from the first 130 subjects were used for development of the initial PPK and PBPK models, and the data collected thereafter were included in the model evaluation/validation data set (**Table S2**).

**Table S1 Risdiplam clinical trials providing PK data for the PBPK, PPK and Mech-PPK modelling**

| Study | Subjects | % of data used in model development: evaluation | Description of studies | Reference |
|---|---|---|---|---|
| NCT02633709 (BP29840) | Healthy male adults (n=26) | 100% : 0% | • Single doses of risdiplam 0.6, 2, 6 or 18 mg<br>• Median of 17 samples for PK assessment per subject | Sturm *et al* [1] |
| NCT03988907 (BP41361) | Healthy adults (n=35) | 0% : 100% | • Single doses of risdiplam 5 mg alone or 8 mg (with midazolam 2 mg single dose on 2 occasions) once daily for 14 days<br>• Median of 38 samples for PK | Cleary *et a l[2]*. |
| NCT03032172 (BP39054) | Type 1, 2 or 3 SMA patients (n=173) | 10% : 90% | • Multiple doses of risdiplam: 0.2,0.25 mg/kg, 3 or 5 mg<br>• Median of 15 samples for PK assessment per patient over median observation period of 90.3 [range: 1-740] days. | Assessment report – Evrysdi [3] |
| NCT02908685 (BP39055) | Type 2 or 3 SMA patients (n=228) | 27% : 73% | • Multiple doses of risdiplam: 0.02,0.05,0.15,0.25 mg/kg, 3 or 5 mg. All patients eventually received 0.25 mg/kg (body weight <20kg) or 5 mg (body weight ≥20 kg).<br>• Median of 20 samples for PK assessment per patient over median observation period of 489 [range: 103-1110] days | Mercuri *et al* [4] |
| NCT02913482 (BP39056) | Type 1 SMA patients (n=62) | 38% : 62% | • Single dose 0.00106 mg/kg (n=1) or multiple doses 0.0106, 0.04, 0.08, 0.2 or 0.25 mg/kg All patients eventually received 0.2 mg/kg ( < 2 years old) or 0.25 mg/kg ( ≥2 years old and body weight <20kg).<br>• Median of 26 samples for PK assessment per patient over median observation period of 483 [range: 1-904] days | Baranello *et al* [5]<br>Darras *et al*. [6] |

Risdiplam solution was given to study subjects by oral administration once daily in all studies.

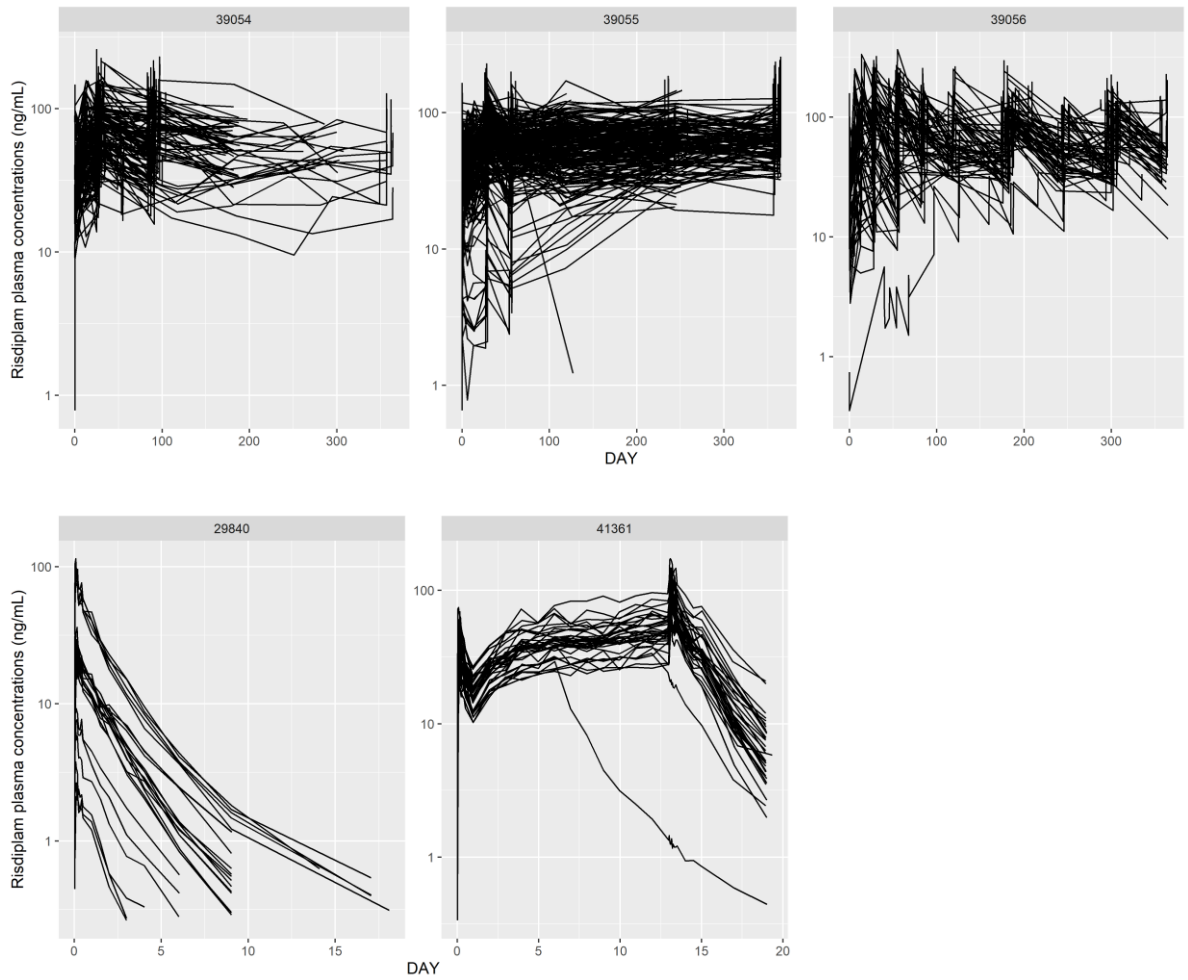


**Fig. S1 Individual plasma concentrations of risdiplam included in the analysis database for the PPK and Mech-PPK modelling**

**Table S2 Summary of number of risdiplam concentrations and demographics of the model development or model evaluation/validation data set.**

| Parameters | Model development | Model evaluation/validation |
|---|---|---|
| **Number of risdiplam data points** | 2492 | 7713 |
| **Number of subjects** | 130 | 395 |
| **Healthy adults: SMA patients** | 26:104 | 35:360 |
| **Sex (male:female)** | 75:55 | 203:192 |
| **Age (year)*** | 7.5 [0.22-52.0] | 13.0 [0.18-61.0] |
| **Body weight (kg)*** | 20.9 [5.0 – 95.3] | 33.7 [4.1-109] |

*at the first dose of risdiplam. Median [range] are shown.

**Definitions of model evaluation and validation:**

- **Model evaluation**: to evaluate the ability of the models to perform simulations for the intended purpose. This includes demonstration of accurate prediction of PK in relevant populations (e.g., goodness-of-fit plots and visual predictive checks).

- **Model validation**: to evaluate whether the model accurately predicts observations from independent data (i.e., not used during model development). The independent data may have been generated for the same compound in different studies or sub-sets of populations.

**Bioanalytical method**

Plasma concentrations of risdiplam were measured by a validated LC-MS/MS method with the quantification limit of 0.25 ng/mL. Calibration range was up to 250 ng/mL using 40 µL plasma aliquots. Accuracy (%RE) and precision (%CV) for risdiplam ranged from -4.3% to 7.0% and from 0.5% to 9.1%, respectively.

## 2. Initial Population PK modelling of risdiplam

A PPK model of risdiplam was initially developed with 2492 risdiplam plasma concentrations collected from 130 subjects (26 healthy adults and 104 SMA patients, Table S2). Multiple compartmental models (1-, 2-, 3- compartment models) and absorption models were evaluated. Ultimately, a structural model with 3-transit compartments for absorption connected to a linear disposition model with 2-compartment was selected. Covariates with time-varying body weight on CL/F, Q/F, Vc/F and Vp/F using allometric function, and time-varying age (maturation function with $E_{max}$ model) on CL/F and Vc/F were included. The estimated allometric coefficient for Vc/F and Vp/F was close to 1 and it was then fixed. It did not increase the objective function significantly.

As summarized in **Table S3**, the PPK model parameters were all estimated with high precision (relative standard errors (RSE) of <30%). Degree of shrinkage were 3.86%, 11.0% and 20.7% for CL/F, Vc/F and ktr, respectively, showing robustness of the *post-hoc* estimates. The goodness-of-fit (GOF) plots (**Fig. S2**) showed good agreement between population or individual predictions and the observations. Conditional weighted residual showed homogeneous distribution against population prediction and time which indicated that the proportional residual error model was adequate. The prediction-corrected visual predictive check (pc-VPC, **Fig. S3**) showed good agreement between the predicted and observed 2.5$^{th}$, median and 97.5$^{th}$ percentile of risdiplam concentrations and indicated an ability of the PPK model to predict the central tendency and inter-individual variability.

**Table S3 Summary of the initial PPK model parameters for risdiplam**

| Parameter | Unit | Estimate | RSE (%) |
|---|---|---|---|
| **Fixed Effects** | | | |
| CL/F | L/h | 3.33 | 4.29 |
| ktr | /h | 4.94 | 3.79 |
| Vc/F | L | 130 | 3.23 |
| Q/F | L/h | 0.85 | 15.1 |
| Vp/F | L | 66.6 | 11.5 |
| **Covariate Effects** | | | |
| Effect of WT on CL/F and Q/F | | 0.418 | 17.2 |
| Effect of WT on Vc/F and Vp/F | | 1.0 fix | NA |
| $Age_{50}$ – CL/F | y | 0.856 | 29.8 |
| $Age_{50}$ – Vc/F | y | 0.308 | 15.6 |
| **Random Effects** | | | |
| CL/F (CV) | | 0.0866 (29.4%) | 14.8 |
| ktr (CV) | | 0.228 (47.7%) | 19.7 |
| Vc/F (CV) | | 0.0591(24.3%) | 16.9 |
| **Error Model** | | | |
| $\sigma_1$ proportional (CV) | | 0.0565(23.8%) | 6.0 |

RSE: relative standard error. CL/F: apparent clearance (CL), ktr: absorption transit rate, Vc/F: apparent central volume of distribution, Q/F: apparent inter-compartmental CL, Vp/F: apparent peripheral volume of distribution, WT: body weight, $Age_{50}$: age to reach 50% of the adult's CL/F or Vc/F. NA: Not applicable. y: year. The median body weight of 38 kg was used for the allometric model for the WT (body weight) effect. The allometric model was defined as follows: $[WT/38]^{0.418}$ for CL/F and Q/F, and $[WT/38]^{1}$ for Vc/F and Vp/F. The maturation functions for CL/F is Age (y)/[Age (y) + 0.856 (y)] and Age (y)/[Age (y) + 0.308 (y)] is for Vc/F

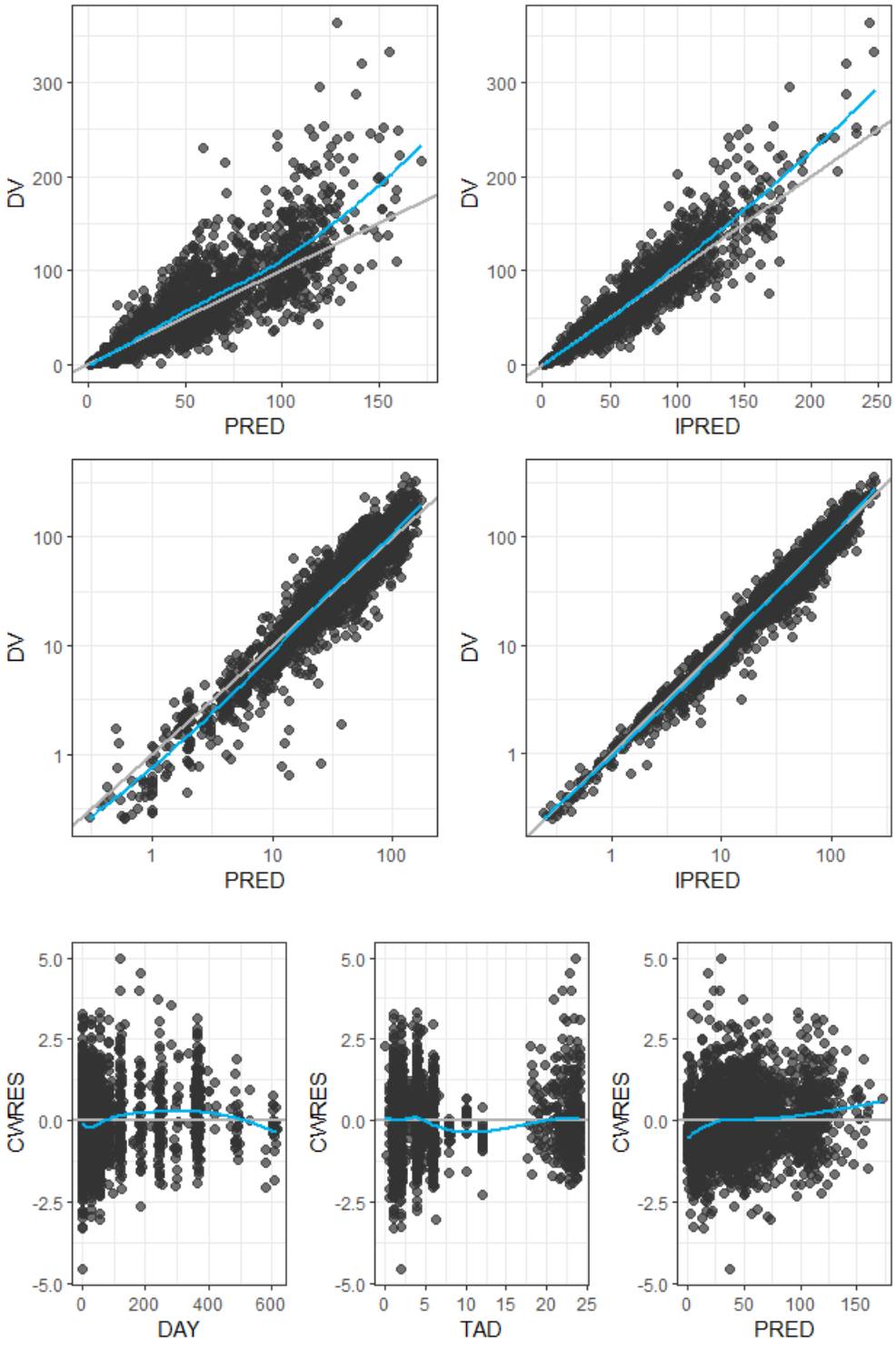


**Fig. S2 Goodness of fit plots of the initial PPK model of risdiplam.**

DV: observed risdiplam concentrations [ng/mL], PRED (IPRED): NONMEM predicted risdiplam concentrations [ng/mL] based on population (individual) PK parameters. CWRES: conditional weighted residual. Gray and blue lines indicate identity and smooth (loess) lines, respectively.

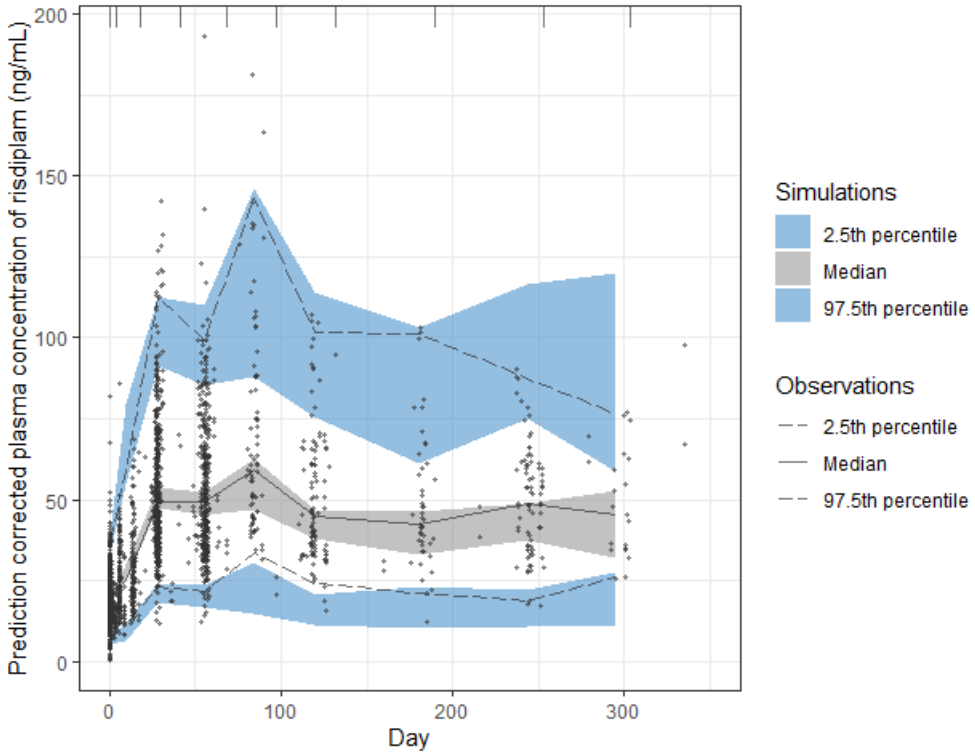


**Fig. S3 Prediction-corrected visual predictive check of the initial PPK model of risdiplam.**

Individual observations corrected by the respective prediction are shown with solid circles. Blue and gray areas present 95% prediction intervals of the 2.5$^{th}$ and 97.5$^{th}$ percentiles of predictions. Dotted and solid lines show 2.5$^{th}$ and 97.5$^{th}$ and median of the observations.

## 3. Adaptation of the PBPK model parameters for SMA patients guided by the *post-hoc* CL/F of the PPK model

### 3.1 PBPK model parameters for adult patients with SMA

The *post-hoc* CL/F estimates of the initial PPK model (**Section 2**) was compared between healthy subjects (n=26) and adult patients with SMA (n=10) who were >18 years old (**Fig. S4**). The geometric mean of the *post-hoc* CL/F was 5.60 L/h in the healthy adults and 3.52 L/h in the adult patients with SMA. This approximately 30% lower CL/F compared to the healthy population was reflected on the $CL_{int}$ and renal CL of the PBPK model for SMA patients as summarized in **Table S4**.

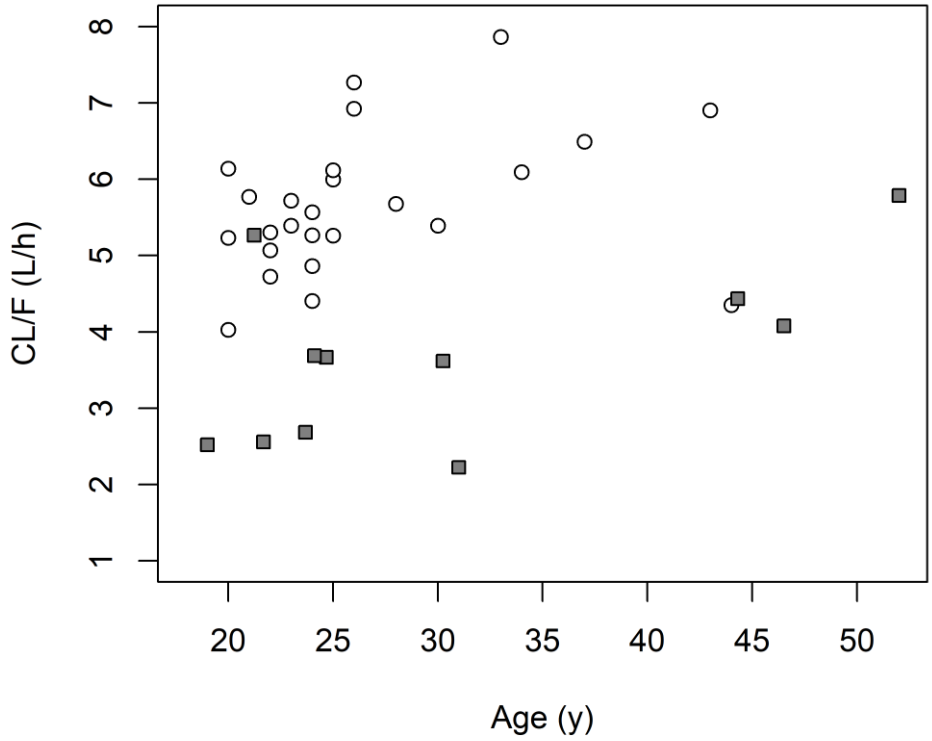


**Fig. S4 Comparisons of *post-hoc* CL/F estimates between healthy adult subjects and adult patients with SMA**

*Post-hoc* CL/F estimates for the healthy adults (open circles) and adult patients with SMA (solid squares) are shown. Origin of these differences are unknown.

**Table S4 Summary of CL parameters of the risdiplam PBPK model for patients with SMA**

| CL | Healthy subjects | Patients with SMA |
|---|---|---|
| **Metabolism** | | |
| $CL_{int,CYP3A4}$ (μL/min/pmol CYP3A) | 0.018 | 0.013 |
| $CL_{int,FMO3}$ (μL/min/pmol FMO3) | 0.36 | 0.27 |
| **Elimination** | | |
| $CL_R$ (L/h) | 0.33* | 0.24 |

*observed in healthy adults [1] and directly included in the PBPK model [7].

### 3.2 Selection of ontogeny functions for the pediatric PBPK model for risdiplam

The *post-hoc* CL/F estimates for 104 SMA patients including pediatric patients aged 2 months to 18 years derived from the initial PPK model (**Section 2**) were normalized by individual body weight to examine age-dependency (**Fig. S5**). The body weight normalized CL/F was higher in pediatric patients than in adult patients with SMA which indicated a higher metabolic activity per gram of liver in children compared to adults. Risdiplam is expected to achieve high bioavailability and is almost exclusively eliminated through hepatic metabolism [7]. Therefore, ontogeny functions which describe increased activity in children compared to adults were necessary for scaling $CL_{int,CYP3A}$ and $CL_{int,FMO3}$ of the pediatric PBPK model of risdiplam. The hepatic CYP3A4 ontogeny functions according to Upreti and Wahlstrom (Upreti function) [8] or Salem et al. (Salem function) [9], and the hepatic FMO3 ontogeny function according to Xu et al. [10] as shown in **Fig. S6** were examined. The PBPK model with implementation of Salem and Xu functions for CYP3A and FMO3, respectively, significantly under predicted risdiplam CL/F (**Fig. S7-A**). Upreti function for scaling both $CL_{int,CYP3A}$ and $CL_{int,FMO3}$ predicted CL/F of risdiplam in pediatric patients aged 2 months to 18 years old more accurately than the other functions and showed good consistency with the *post-hoc* CL/F by the PPK model (**Fig. S7-B**).

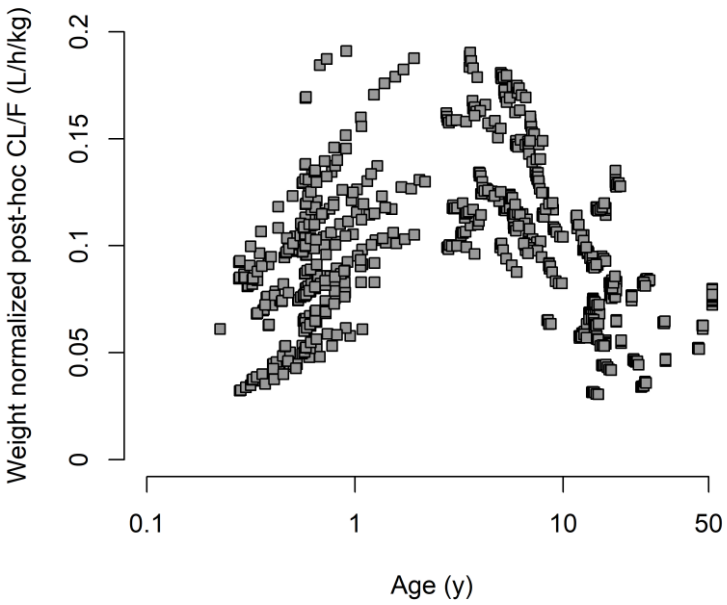


**Fig. S5 Distribution of *post-hoc* CL/F normalized by body weight for the age range of the patients with SMA**

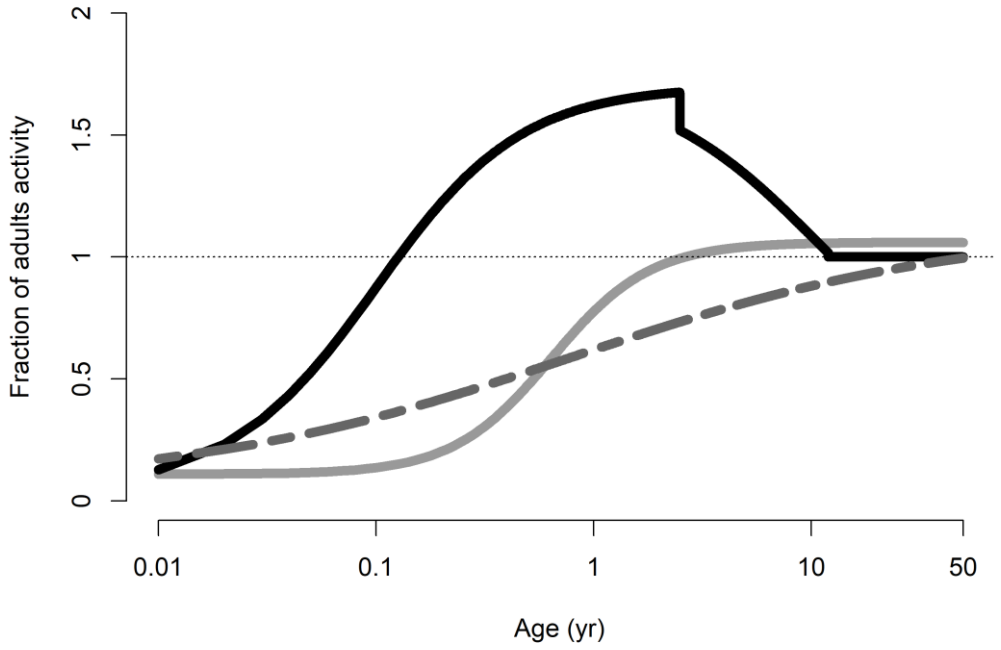


**Fig. S6 Hepatic CYP3A and FMO3 ontogeny functions considered for the pediatric PBPK model of risdiplam.**

The hepatic CYP3A ontogeny function according to Upreti and Wahlstrom [8] (black solid line) or Salem *et al* [9]. (gray solid line) and the hepatic FMO3 ontogeny function according to Xu *et al*. [10] (gray dash line) are shown.

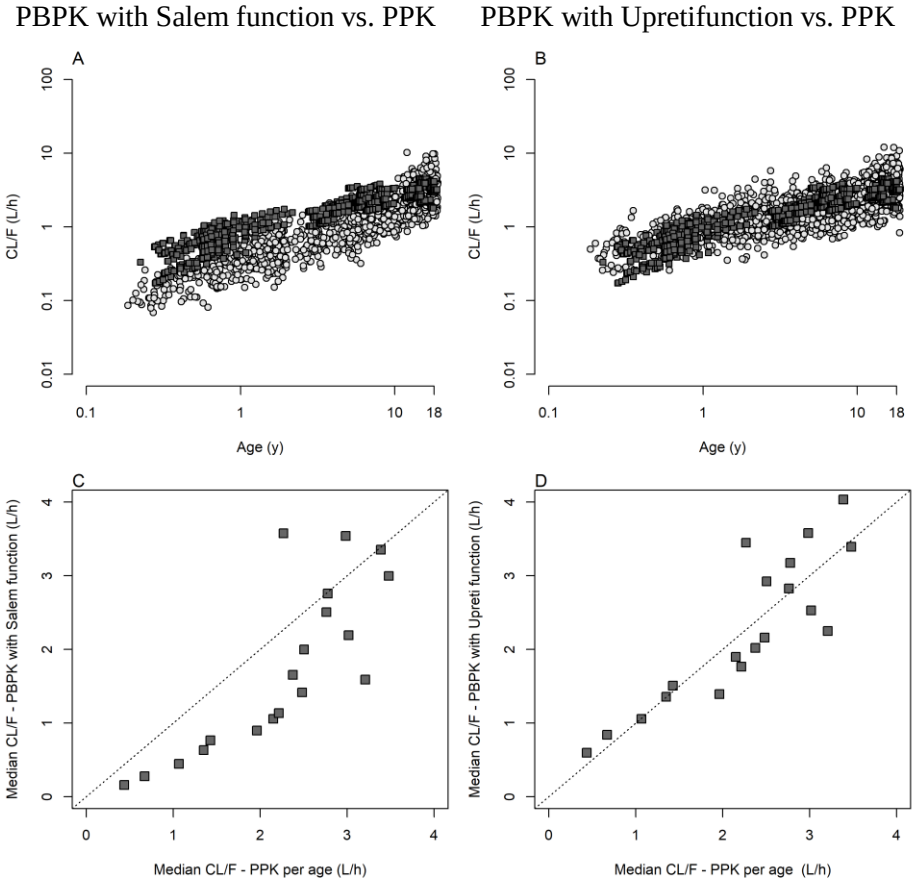

**Fig. S7 Comparisons of distribution of CL/F predicted by the PBPK model (left: with Salem function, right: with Upreti function) and *post-hoc* estimates of CL/F in the pediatric patients with SMA.**

Risdiplam CL/F predicted for the pediatric patients with SMA aged 2 months to 18 years old by the PBPK model with implementation of (A) Salem function [9] for the hepatic CYP3A and the FMO3 ontogeny based on the *in vitro* investigations [10-12] or (B) Upreti function [8] for the hepatic CYP3A and FMO3 ontogeny. The risdiplam CL/F predicted by the PBPK models are shown with gray circles and the individual *post-hoc* CL/F estimates by the PPK model (**Section 2**) are shown with solid dark gray squares. Median of CL/F per age group (0.5-1 year old group following by approximately 1 year interval per group until 19 years old) were compared between the *post-hoc* CL/F estimates by the PPK model and the PBPK models with Salem function (C) or with Upreti function (D). The dotted line shows line of unity.

## 4. Physiological data and CL model used for investigation of in vivo FMO3 ontogeny.

Physiological parameters such as liver weight and blood flow were individually calculated according to all available time-varying age, body weight and height collected from individual patients throughout the observation period.

**Body surface area (BSA)**

BSA was required for the estimation of liver weight, blood flow and glomerular filtration rate (GFR). BSA was calculated according to DuBois and DuBois [13] if body weight was greater than 15 kg and Haycock et al [14] if body weight was less than 15 kg to align the approach taken by Johnson et al [15].

**BSA for subjects with body weight > 15 kg:**

$$BSA\ (m^2) = 0.007184 \times BW\ (kg)^{0.425} \times Height\ (cm)^{0.725}$$ **Equation S1**

**BSA for subjects with body weight ≤ 15 kg:**

$$BSA\ (m^2) = 0.024265 \times BW\ (kg)^{0.5378} \times Height\ (cm)^{0.3964}$$ **Equation S2**

**Liver weight**

Individual liver weight was calculated according to the following equation and the liver density of 1.08 g/L was assumed as in SimCYP pediatric module version 20.

$$Liver\ volume\ (L) = 0.722 \times BSA^{1.176}$$ **Equation S3**

**Glomerular filtration rate (GFR)**

Age dependent GFR was according to Johnson *et al.* which has been verified by external data [15].

$$\text{GFR (mL/min)} = (-6.1604 \times BSA^2) + (99.054 \times BSA) - 17.74$$ **Equation S4**

**Microsomal protein per gram of liver (MPPGL)**

The following equation according to Barter *et al*. [16] was used for calculation of MPPGL.

$$\text{MPPGL (mg/g)} = 10^{(1.407+0.0158\times Age-0.00038\times Age^2+0.0000024\times Age^3)}$$ **Equation S5**

The calculated MPPGL of 2 months and 18 years old patients according to this equation are 26 and 38 mg/g liver, respectively. These values are in agreement with the recent report by Leeder et al. where the mean ± SD of 30.4 ± 1.7 mg/g liver was reported as the representative MPPGL value between one month postnatal age and early adulthood based on the analysis of 160 liver samples collected from 129 pediatric and 31 adult donors [17].

**Liver blood flow ($Q_H$)**

Total liver blood flow represents the sum of hepatic arterial and portal vein blood flows, corresponding to 6.5% and 19% (male and 21.5% for female) of cardiac output, respectively. The cardiac output was estimated according to SimCYP version 20 as follows:

$$\text{Cardiac output} = BSA \times (194.15 + 4046.7 \times (\exp^{(-0.2117\times Age)} - \exp^{(-0.224\times Age)}))$$ **Equation S6**

This model has been verified by data reported by Guyton and Hall [18] and ICRP 2002 [19].

**Unbound fraction in plasma ($fu_p$)**

The $fu_p$ was measured in all pediatric SMA patients <12 years and used in the modelling, otherwise 11% was assumed for all other subjects [20]. Measured haematocrit values were used for scaling blood to plasma partition coefficient (BP).

**Definition of CL model for the Mech-PPK model to estimate *in vivo* FMO3 ontogeny function**

The Mech-PPK model of risdiplam included a mechanistic hepatic intrinsic clearance and bioavailability terms according to the well-stirred liver model (Equation S7 and Equation S8, respectively). Total plasma CL after inclusion of renal CL ($CL_R$) is according to Equation S9. Renal clearance ($CL_R$) was scaled for pediatric patients by age-dependent glomerular filtration rate [15].

$$\boldsymbol{Hepatic\ blood\ CL\ (CL_{HB})} = \frac{Q_H \times f_{uB} \times CLu_H}{Q_H + f_{uB} \times CLu_H} \qquad \textbf{Equation S7}$$

$$\boldsymbol{Bioavailability\ (F)} = F_H = 1 - \left(\frac{CL_{HB}}{Q_H}\right) \qquad \textbf{Equation S8}$$

$$\boldsymbol{Total\ plasma\ CL\ (CL)} = CL_{HB} \times BP + CL_R \qquad \textbf{Equation S9}$$

where $Q_H$ is hepatic liver blood flow as defined above and $f_{uB}$ is an unbound fraction in blood defined as unbound fraction in plasma ($f_{uP}$) divided by blood to plasma partition coefficient (BP).

The $CL_{uH}$ was defined by Equation S10 using liver weight and MPPGL as defined above.

$$CLu_H = (CL_{int,FMO3} + CL_{int,CYP3A}) \times Liver\ weight \times MPPGL \qquad \textbf{Equation S10}$$

The $CL_{uH}$ of risdiplam in adults were estimated using the data set limited to adult population (i.e. no ontogeny function) and the geometric mean for the healthy adults and adult patients with SMA were separately calculated. The 20% of the respective geometric mean was set as $CL_{int,CYP3A\ in\ adults}$ ($fm_{CYP3A}$=20%) and the rest was assigned to $CL_{int,FMO3\ in\ adults}$ ($fm_{FMO3}$=75%). The age-dependent $CL_{int,Enzyme}$ ($CL_{int,Enzyme\ in\ children}$) for individual enzyme was defined as a function of $CL_{int,Enzyme\ in\ adults}$ and the respective ontogeny functions (Equation S11). The hepatic CYP3A ontogeny was fixed to the model according to Upreti and Wahlstrom [8] and six structural models for the *in vivo* FMO3 ontogeny (Table 1) were investigated.

$$CL_{int,Enzyme\ \textbf{in children}} = CL_{int,\textbf{Enzyme in adults}} \times Ontogeny_{Enzyme} \qquad \textbf{Equation S11}$$

## 5. Final PPK model parameters and Goodness-of-Fit Plots

The goodness-of-fit (GOF) plots of the final PPK model of risdiplam in subjects ≥2 months old (10,205 observations from 525 subjects) are shown in **Fig. S8**.

Although the PPK model parameters were shifted from the initial PPK model (**Table S3**), the population estimates of CL/F and Vc/F, critical parameters to predict PK, were consistent in children aged 2 months to 10 years old (**Fig. S9**) between these models. It supports robustness of the initial PPK model. The estimated allometric exponent of 0.276 for risdiplam CL/F was lower than the commonly assumed value of 0.75 based on metabolic rates. The maturation function with $Age_{50}$ of 0.877 years old means that 70% of CL/F maturation would be achieved by the age of 2 years, which is an indication of higher body weight normalized CL/F in children as depicted in **Fig. S10**. The final PPK model parameter estimation step was repeated with an additional residual error for the venous samples collected from healthy subjects. The estimated residual error of SMA patients was marginally increased from 23.4% (Table 2) to 24.7% when the samples from the healthy subjects were separated, indicating minimum impact of the healthy subjects' data on the evaluation of residual error of the SMA patients.

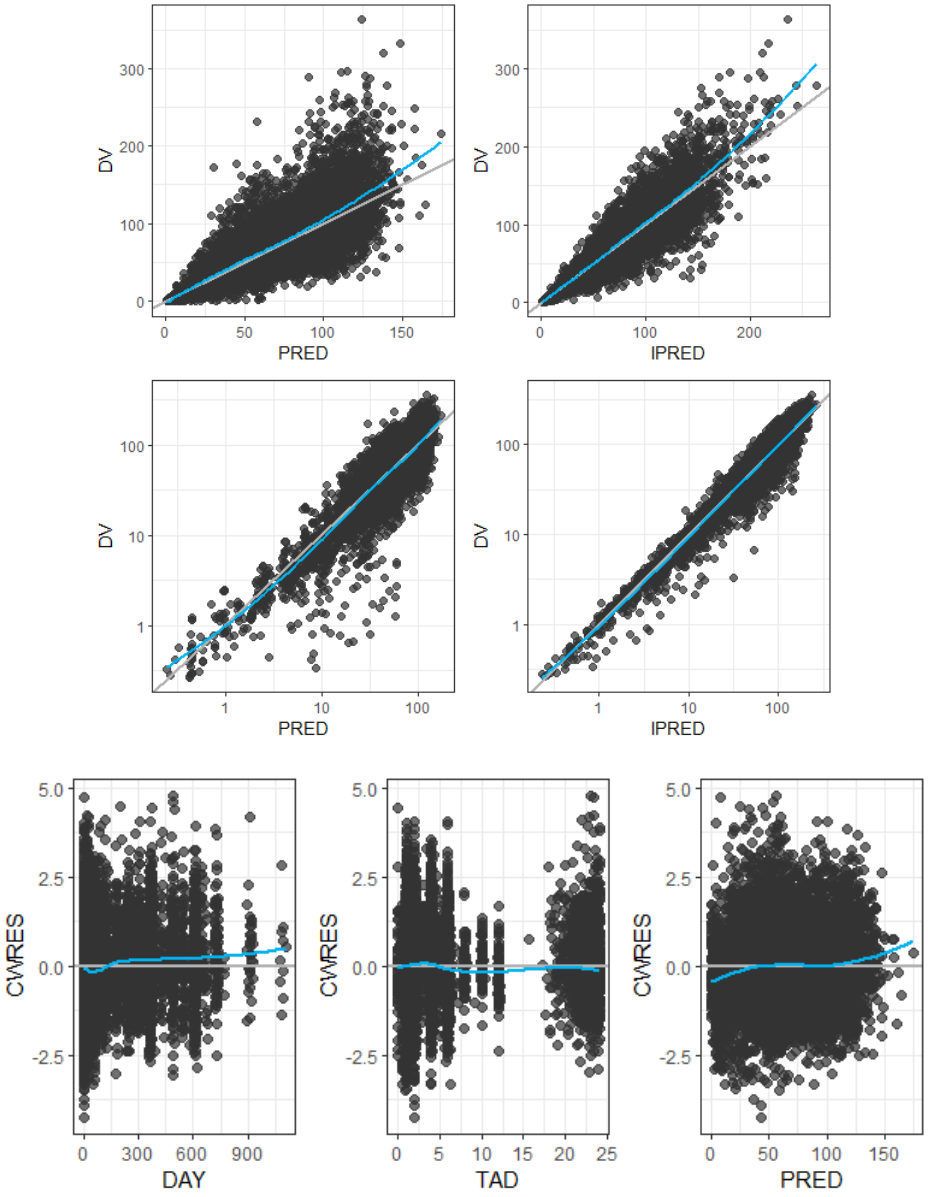

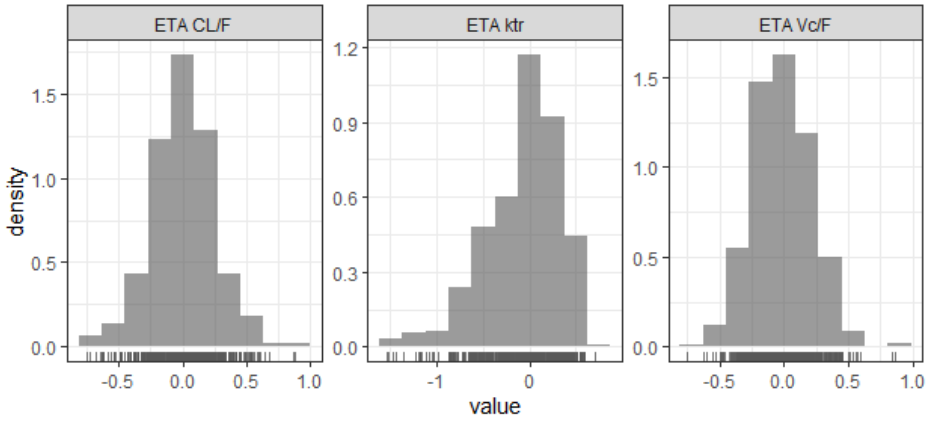


**Fig. S8 Goodness of fit plots of the final PPK model of risdiplam.**

DV: observed risdiplam concentrations [ng/mL], PRED (IPRED): NONMEM predicted risdiplam concentrations [ng/mL] based on population (individual) PK parameters. CWRES: conditional weighted residual. Gray and blue lines indicate identity line and smooth, respectively. CL/F: apparent clearance, ktr: transit absorption rate and Vc/F: apparent central volume of distribution.

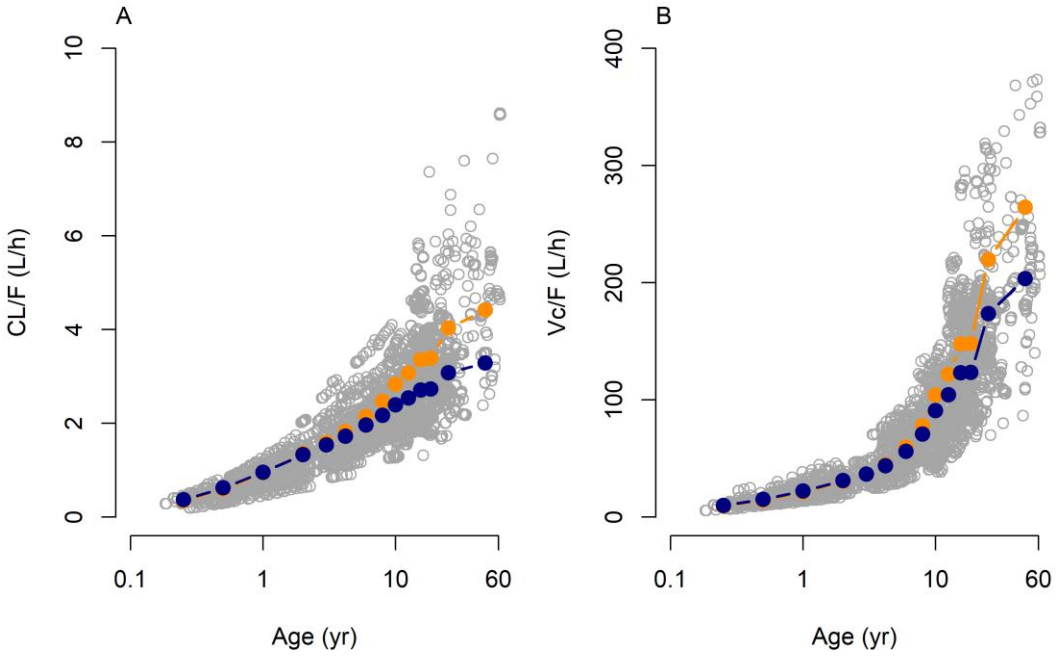


**Fig. S9 Comparisons of the population estimates of CL/F (A) and Vc/F (B) by the initial and the final PPK models**

The *post-hoc* CL/F and Vc/F of the final PPK model (open grey circle) are shown overlaid the typical CL/F and Vc/F of each age group using the initial (orange circles and lines) and the final (navy circles and lines) PPK models. Actual age and median body weight for each age group of the final data base were used for the calculation of the typical estimates.

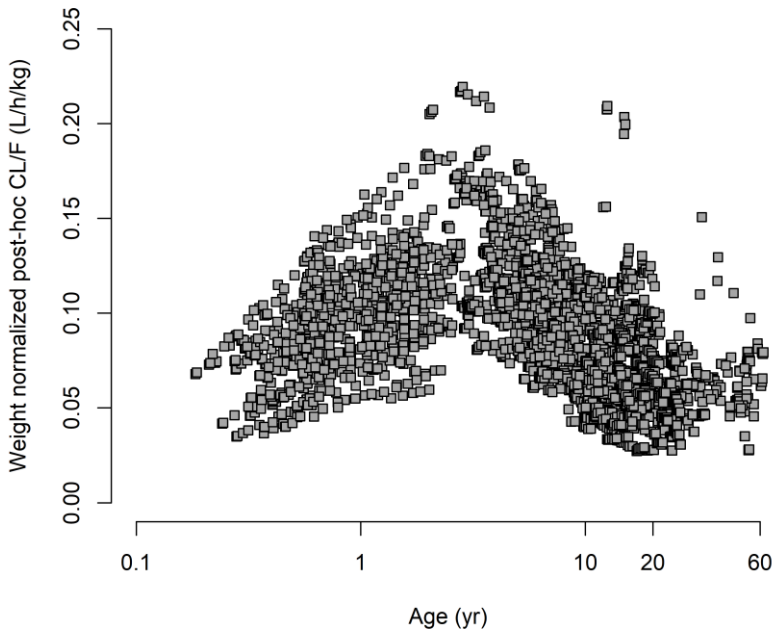


**Fig. S10 Distribution of *post-hoc* CL/F of the final PPK model normalized by body weight for the age range of the patients with SMA**

## 6. Validation of the PBPK model with independent data set

**PBPK model for adult patients with SMA**

Simulation of risdiplam PK after 5 mg once daily dosing for 14 days was performed with the virtual population (n=400) and predicted risdiplam CL/F and exposure parameters ($AUC_{0\text{-}24h}$ and $C_{max}$) by the PBPK model for adult SMA patients. The predictions were compared to the individual *post-hoc* CL/F of the PPK model, the observed $C_{max}$ and the AUC estimated using the *post-hoc* parameters of the PPK model (**Section 5**) of the 71 adult SMA patients in the model evaluation/validation data set (**Table S2**).

The predicted risdiplam CL/F by the PBPK model showed good agreement with the *post-hoc* CL/F for the adult SMA patients estimated by the *post-hoc* CL/F of the PPK model as shown in **Fig. S11**. There was no age dependency in CL/F in this population. Although over-prediction of variability by the PBPK model was shown, the median of $AUC_{0\text{-}24h}$ and $C_{max}$ were in good agreement with the observations (**Fig. S12**) and they were both within 0.8-1.25 of the observations.

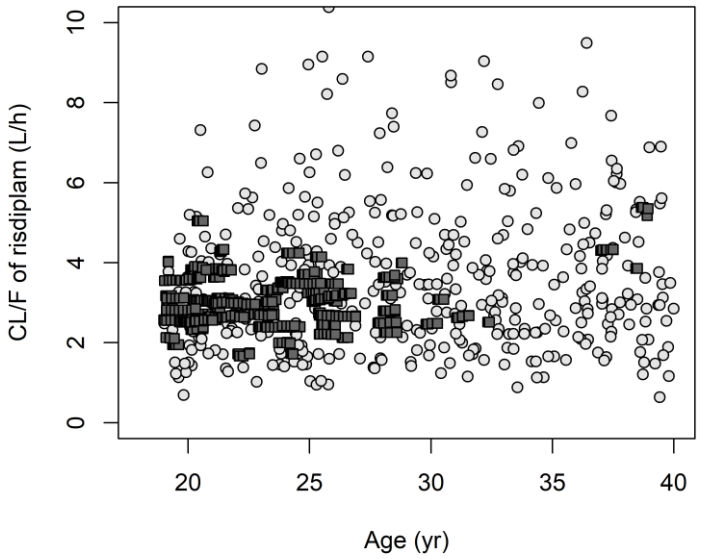


**Fig. S11 Comparison of the predicted risdiplam CL/F by the PBPK model and the individually estimated post-hoc CL/F by the PPK model for the adult SMA patients of the validation data set**

The risdiplam CL/F predicted by the PBPK model are shown with gray circles and the individual *post-hoc* CL/F estimates by the PPK model (**Section 5**) are shown with solid dark gray squares.

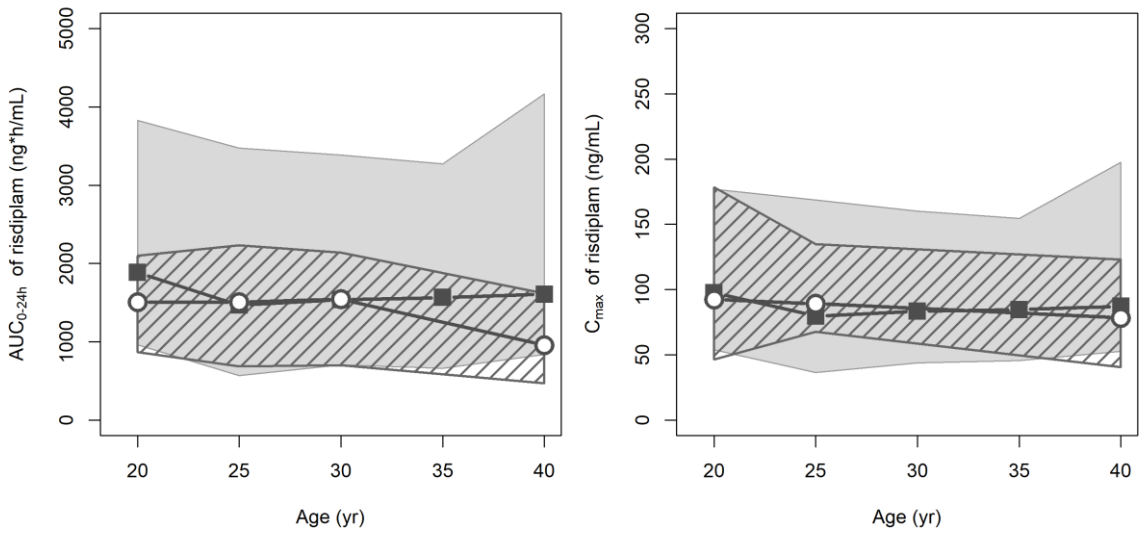


**Fig. S12 Comparison of predicted and observed risdiplam $AUC_{0\text{-}24h}$ and $C_{max}$ of the adult SMA patients of independent data set**

Geometric means of simulated (solid squares) and observed (open circles) $AUC_{0\text{-}24h}$ and $C_{max}$ are shown. The grey and striped shapes show 90% prediction interval or 5th-95th percentiles of the observations, respectively.

**The PBPK model for pediatric patients with SMA**

Simulation of risdiplam PK after 0.2 mg/kg for 2 months to 2 years, 0.25 mg/kg for patients ≥2 years and weighing <20 kg or 5 mg for patients ≥2 years and weighing ≥20 kg once daily [21] was performed to predict risdiplam CL/F and exposure parameters ($AUC_{0\text{-}24h}$ and $C_{max}$) for pediatric patients aged between 2 months to 18 years old (n=1800).

Age and risdiplam CL/F relationship predicted by the pediatric PBPK model showed good agreement with the *post-hoc* CL/F estimates of the final PPK model (**Section 5**) for the 289 SMA patients aged 2 months to 18 years of the evaluation/validation data set (**Fig. S13**). The geometric mean of predicted $AUC_{0\text{-}24h}$ (**Fig. 2-B**) and $C_{max}$ (**Fig. S14**) were generally consistent and within 0.8-1.25-fold of the observations of the pediatric patients with SMA except for 2-4 years old (AUC ratio=1.4 and $C_{max}$ ratio = 1.5).

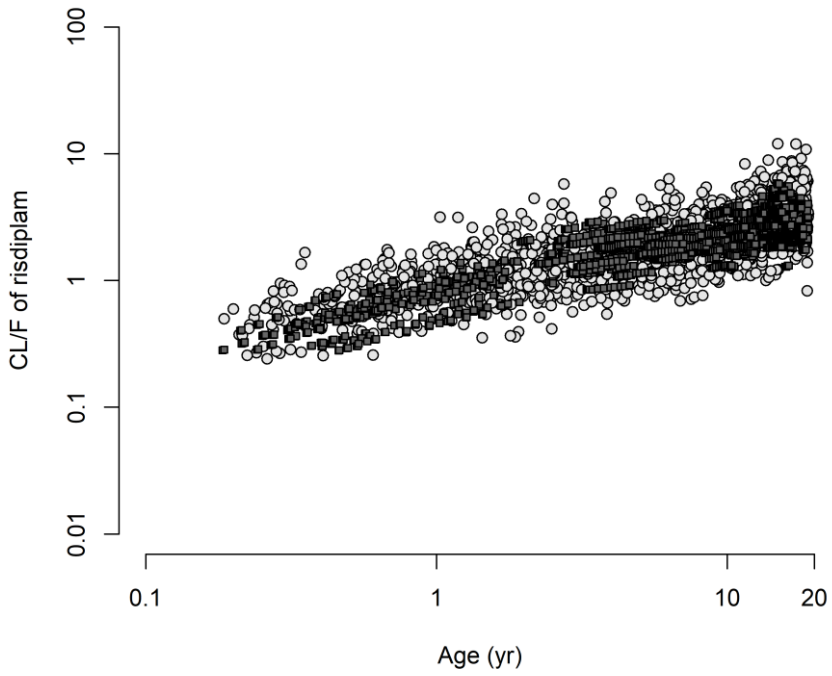


**Fig. S13 Comparison of the predicted risdiplam CL/F by the PBPK model and the individually estimated *post-hoc* CL/F by the PPK model for the pediatric patients with SMA included in the validation data set**

Risdiplam CL/F predicted by the pediatric PBPK model with implementation of Upreti function for the hepatic CYP3A and FMO3 ontogeny (grey circles) are compared with the individual *post-hoc* CL/F estimates (grey squares) for 289 pediatric patients with SMA aged 2 months and 18 years by the final PPK model (Table 2).

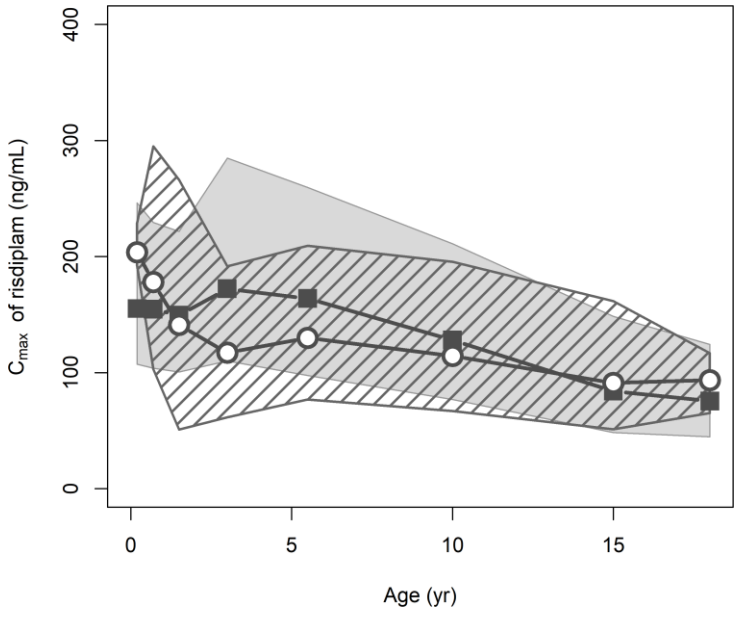


**Fig. S14 Comparison of predicted and observed risdiplam $C_{max}$ of the independent data set**

Geometric means of simulated (solid squares) and observed (open circles) $C_{max}$ are shown. The gray and striped shapes show 90% prediction interval or 5th-95th percentiles of the observations, respectively. Geometric means of the simulated risdiplam $C_{max}$ were all within 0.8-1.25 fold of the observations of 286 pediatric patients with SMA who received the approved risdiplam dose [21] except for 2-4 years (1.5).

## 7. Goodness-of-fit plots of the mechanistic PPK model of risdiplam with FMO3 ontogeny function with Model 6

The estimated *in vivo* FMO3 ontogeny Model 6 and its 95% confidence interval derived by bootstrap with 200 estimations are shown in Fig. S15. Goodness-of-fit (GOF) plots of the Mech-PPK model with Model 6 for the *in vivo* FMO3 ontogeny are shown below. Population and individual predictions were generally in a good agreement with the observations. Distribution of conditional weighted residual (CWRES) for the range of time (after the first or last doses) and population predictions were homogenous. ETAs of CLint, ktr and Vc were generally normally distributed with median of 0.

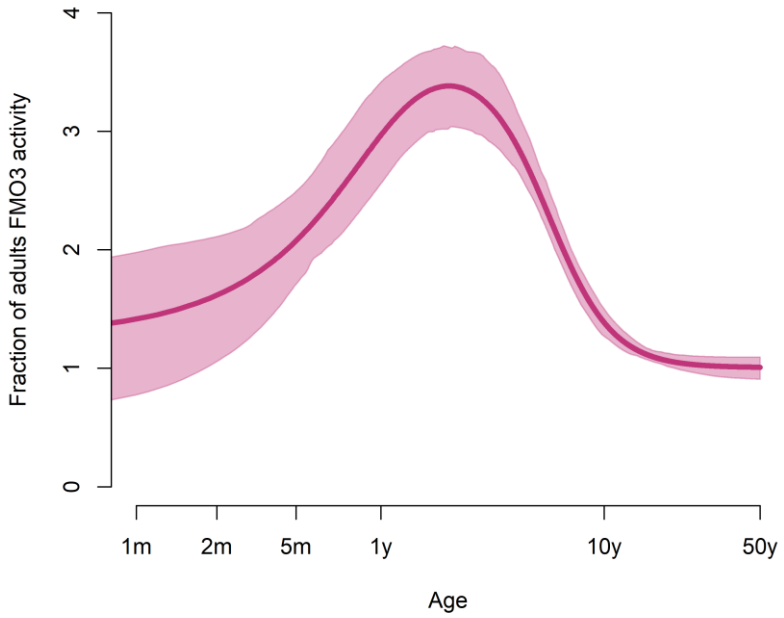


**Fig. S15 *in vivo* FMO3 ontogeny Model 6 estimated by the mechanistic PPK model of risdiplam and 95% confidence interval.**

Predictions of *in vivo* FMO3 ontogeny (solid magenta line) and 95% confidence interval (magenta shade: 2.5$^{th}$ to 97.5$^{th}$ percentiles of predicted fraction of adults FMO3 activity by bootstrap analyses) between 2 months and 50 years old are shown.

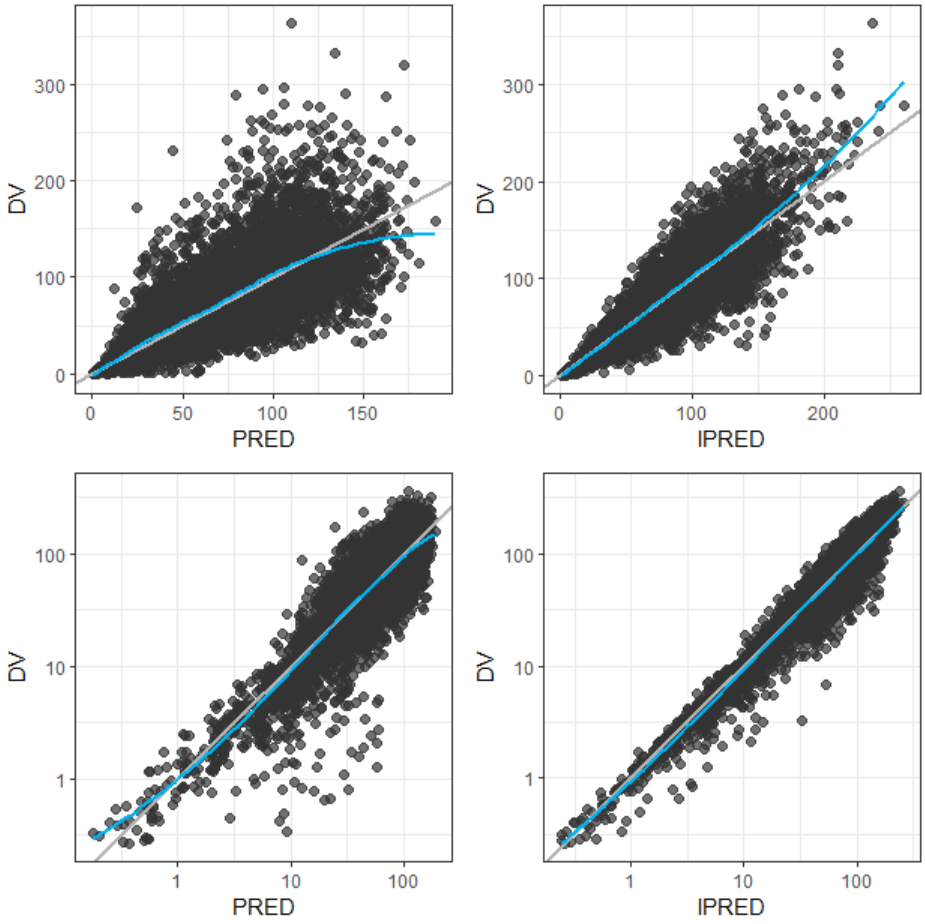


**Fig. S16 Goodness-of-fit (GOF) plots of the Mech-PPK model with Model 6**

DV: observed risdiplam concentrations [ng/mL], PRED (IPRED): NONMEM predicted risdiplam concentrations [ng/mL] based on population (individual) PK parameters. Gray and blue lines indicate identity line and smooth, respectively.

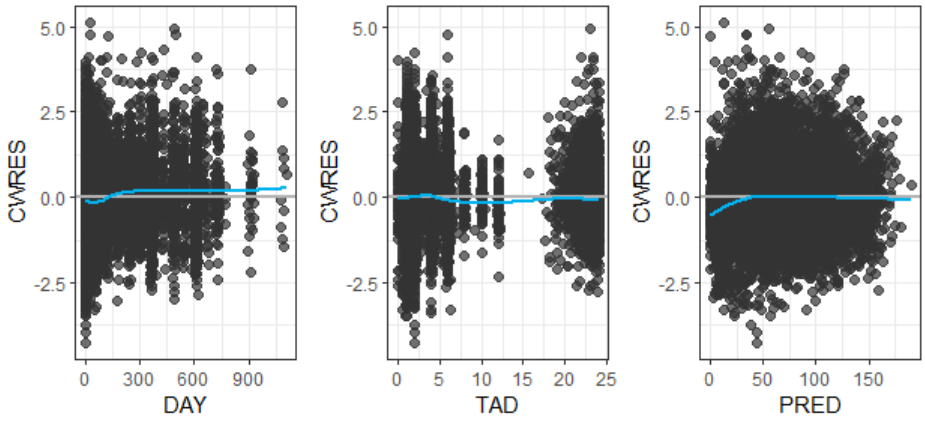


**Fig. S17 Distribution of conditional weighted residuals**

CWRES- conditional weighted residual. CWRES are plotted against time after the first (day) or last (hours) doses. Blue lines indicate smooth.

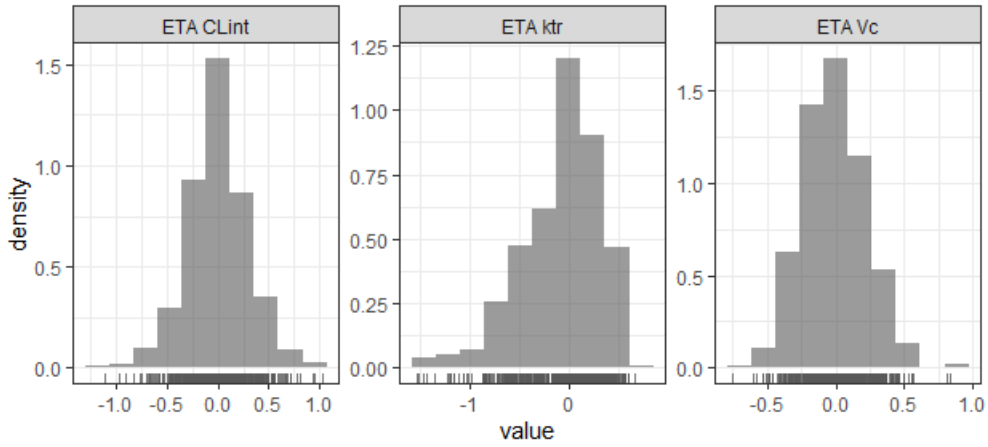


**Fig. S18 ETA distributions**

Histograms of ETA of $CL_{int}$ (intrinsic CL) which was applied for $CL_{int,\ CYP3A}$ and $CL_{int,FMO3}$, ETA of ktr (transit absorption rate) and ETA of Vc (central volume of distribution)

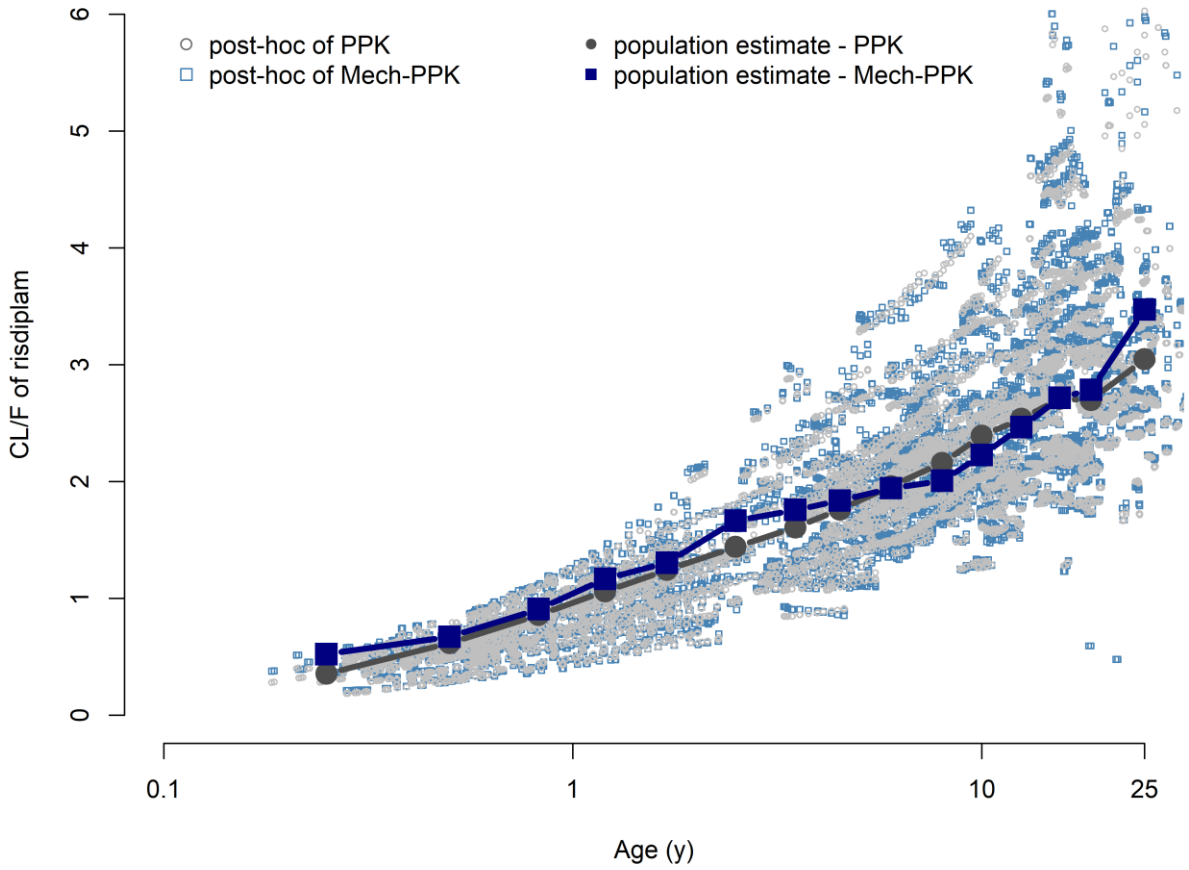


**Fig. S19 Comparisons of the predicted risdiplam CL/F by the PPK and Mech-PPK models**

The *post-hoc* estimates of CL/F by the PPK (gray open circles) and Mech-PPK (blue open squares) models are compared with the population estimates by the corresponding models. The population estimates of risdiplam CL/F by the PPK model (gray solid line and circles) were calculated using median age and body weight of the actual SMA patients. In addition, median of estimated hepatic blood flow, liver weight, microsomal protein per gram of liver, unbound fraction in blood of each age group of the pediatric SMA patients were considered for the population estimate of risdiplam CL/F by the Mech-PPK model (navy solid line and squares).

## 8. Prediction of risdiplam Cmax in pediatric patients with SMA by the updated pediatric PBPK model with the estimated *in vivo* FMO3 ontogeny function.

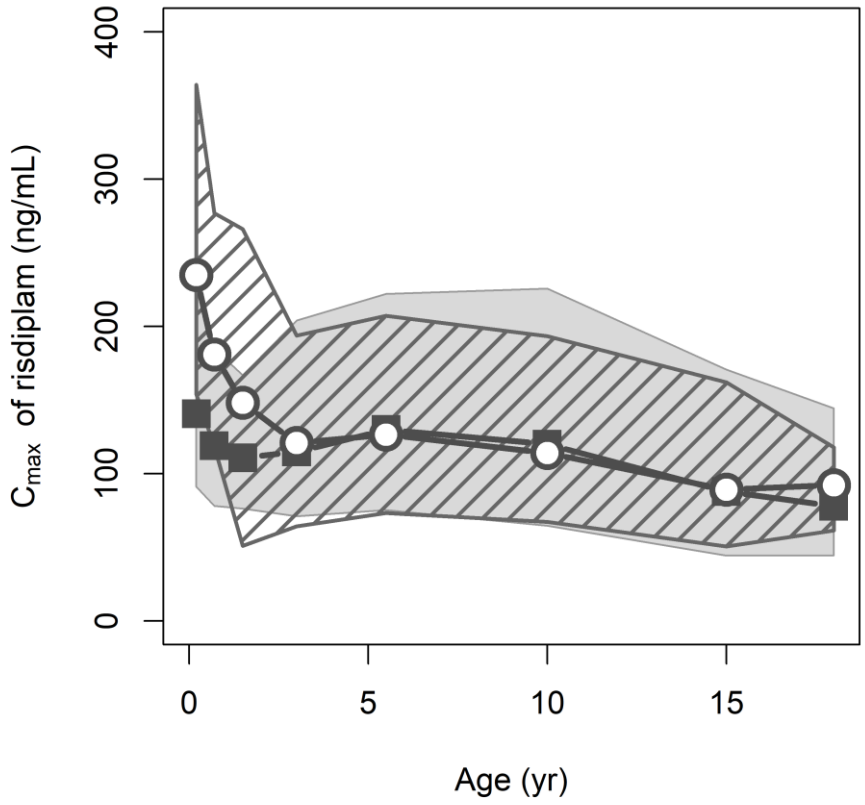


**Fig. S20 Evaluation of predicted risdiplam Cmax in pediatric patients with SMA by the updated pediatric PBPK model with the estimated in vivo FMO3 ontogeny (Model 6).**

Prediction of risdiplam $C_{max}$ by the updated pediatric PBPK model with the estimated *in vivo* FMO3 ontogeny function was compared with the observation of 361 pediatric patients with SMA. A customized demographic model for SMA patients [2] was used. The gray and striped shapes show 90% prediction interval or $5^{th}$-$95^{th}$ percentiles of the observations, respectively. Geometric means of simulated (solid squares) and observed (open circles) values are shown. Geometric means of the simulated risdiplam $C_{max}$ were 0.6 to 0.75-fold of the observations in children aged 2 months to 2 years old and within 0.8-1.25 fold in children aged 2 to 18 years old.

## 9. CYP3A DDI assessment in children with the newly estimated *in vivo* FMO3 ontogeny function

### 9.1 Risdiplam – CYP3A victim DDI prediction

The $fm_{CYP3A}$ of risdiplam is approximately 20% and therefore CYP3A-victim DDI risk is low. The $fm_{CYP3A}$ of risdiplam in children was predicted by the pediatric PBPK models. The predicted $fm_{CYP3A}$ of risdiplam in children aged 2 months to 18 years old using the validated pediatric PBPK model (**Section 6**) where Upreti function was applied for both CYP3A and FMO3 ontogeny (**Fig. S21-A**) was consistently at around 20% across the age range (**Fig. S21-B**). This trend is due to the parallel development of CYP3A and FMO3 assumed in the model. The updated PBPK model with the estimated *in vivo* FMO3 ontogeny function Model 6 (**Fig. S21-C**) predicted lower $fm_{CYP3A}$ of risdiplam in children <10 years old (**Fig. S21-D**), reflecting increased FMO3 contribution to risdiplam metabolism due to higher relative FMO3 expression/activity in children compared to adults than that predicted by Upreti functions in this age range.

**Upreti function for both CYP3A and FMO3** | **Upreti function for CYP3A and the newly estimated *in vivo* FMO3 ontogeny**

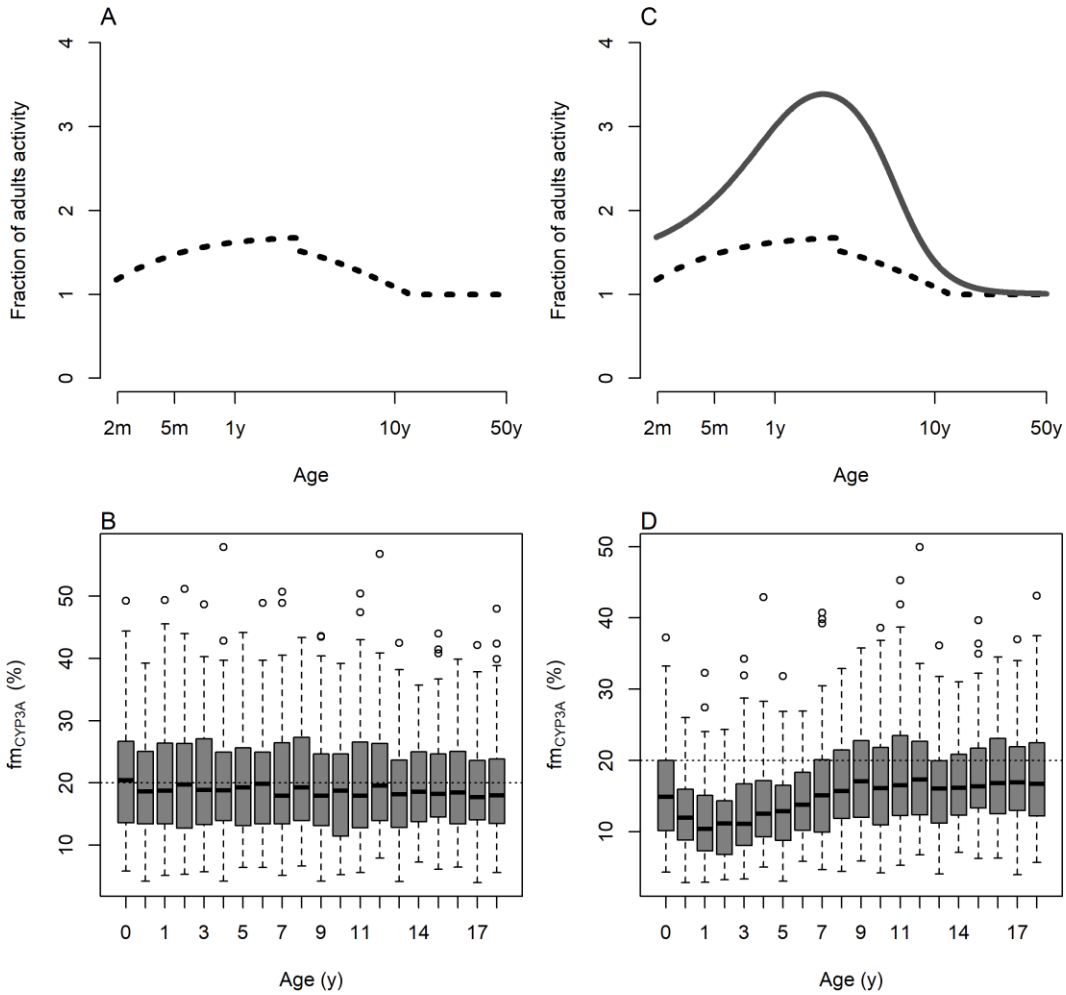


**Fig. S21 Ontogeny functions of CYP3A and FMO3, and the predicted $fm_{CYP3A}$ of risdiplam**

The predicted $fm_{CYP3A}$ of risdiplam using the validated pediatric PBPK model of risdiplam with Upreti function (dotted lines in **A** and **C**) for both hepatic CYP3A and FMO3 ontogeny (**B**) or by using the estimated *in vivo* FMO3 ontogeny (Model 6, solid line in **C**) in the updated pediatric PBPK model (**D**).

## 9.2 Prediction of time-dependent inhibition of CYP3A of risdiplam

Risdiplam exhibited time-dependent inhibition (TDI) of CYP3A with $K_I$=13 µM and $k_{inact}$=3.9/h *in vitro* with human liver microsomes [7]. Risdiplam 8 mg once daily for 14 days increased midazolam AUC and $C_{max}$ by 11% and 16% in healthy adults, respectively [2]. The results of this clinical DDI study in healthy adults were previously extrapolated to children aged 2 months to 18 years old by the validated PBPK model which indicated low TDI propensity (i.e., fold increase in midazolam AUC and $C_{max}$ <1.25) [2]. The TDI prediction was repeated with the updated pediatric PBPK model with the estimated *in vivo* FMO3 ontogeny function Model 6 (**Fig. S22**).

The DDI simulation was performed for pediatric patients aged 2 months to 18 years old (n=2000) assuming the same study design as the previous prediction [2]: oral administration of midazolam 0.1 mg/kg before and after 13 days treatment of risdiplam 0.2 mg/kg for 2 months to 2 years, 0.25 mg/kg for patients ≥2 years and weighing <20 kg or 5 mg for patients ≥2 years and weighing ≥20 kg once daily [21]. On day 13, midazolam was given 1 hour after risdiplam administration.

The major site of inhibition for risdiplam is intestine [2], and therefore, change in the hepatic FMO3 ontogeny was not expected to alter the prediction of TDI effect on the midazolam PK. Indeed, the predicted midazolam AUC and $C_{max}$ ratios were consistently low with the geometric mean <1.25 across age range and 95$^{th}$ percentile of the predictions were well below 2-fold (**Fig. S22**).

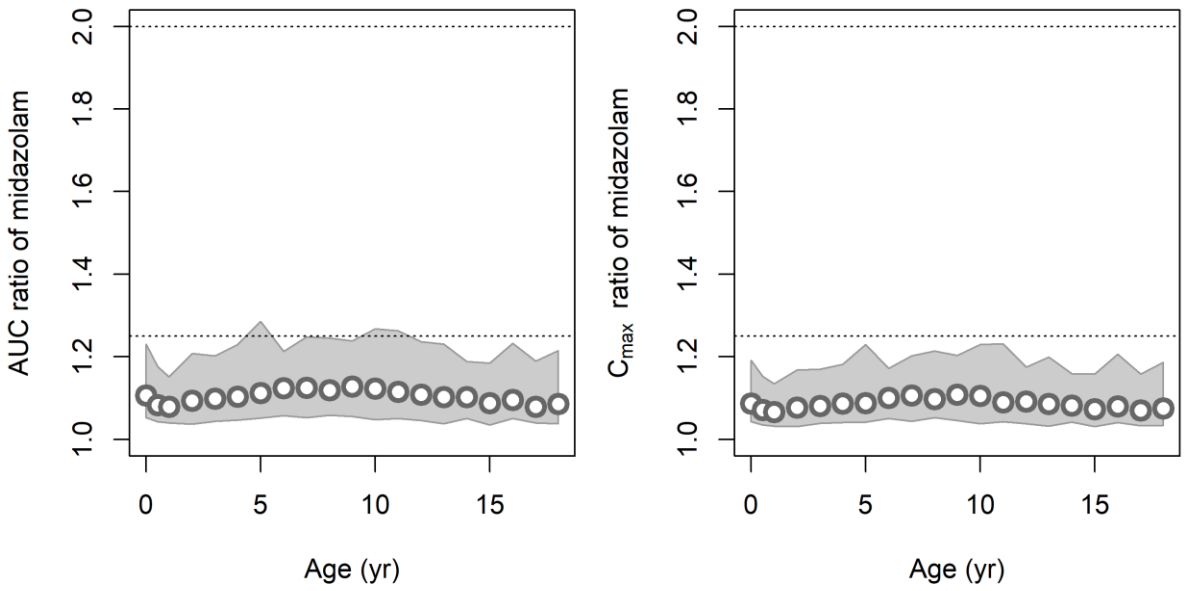


**Fig. S22 Predicted AUC and $C_{max}$ ratios of midazolam in the presence of risdiplam in pediatric SMA patients aged 2 months to 18 years using the estimated *in vivo* FMO3 ontogeny functions.**

Geometric mean (open circles) and 90% prediction intervals (gray shade) are shown. For these simulations, Upreti and Johnson functions for the hepatic and intestinal CYP3A ontogeny functions, respectively and risdiplam TDI parameters refined by *in vivo* data were used [2].

## 9.3 Impact of uncertainty in FMO3 ontogeny on predictions of CYP3A-victim DDI and –TDI propensity in infants aged 2 to 4 months old.

### 9.3.1 Risdiplam

The predictions of FMO3 activity were variable in infants <4 months old among the six estimated ontogeny models (Figure 3). Therefore, the impact of uncertainty of FMO3 ontogeny in infants aged 2 months (the youngest observation of the applied database) to 4 months old on CYP3A-mediated DDI predictions for risdiplam was evaluated. In addition to Model 6, two other estimated *in vivo* FMO3 ontogeny models which predict the lowest (Model 3) and the highest (Model 2) FMO3 activity (**Fig. S23-A**) were applied for the CYP3A-mediated DDI predictions.

**Model 2:** $$\mathbf{1.98} + \frac{(\mathbf{3.36} - \mathbf{1.98}) \cdot \boldsymbol{Age}^{\mathbf{5.01}}}{(\boldsymbol{Age}^{\mathbf{5.01}} + \mathbf{0.675}^{\mathbf{5.01}})} \times (\mathbf{1} - \mathbf{1.69} \times \frac{\boldsymbol{Age}^{\mathbf{3.40}}}{(\boldsymbol{Age}^{\mathbf{3.40}} + \mathbf{5.95}^{\mathbf{3.40}})})$$ **Equation S12**

**Model 3:** $$\left(\mathbf{15.3} \times \frac{\boldsymbol{Age}^{\mathbf{0.683}}}{\boldsymbol{Age}^{\mathbf{0.683}} + \mathbf{2.69}^{\mathbf{0.683}}}\right) \times \left(\mathbf{1} - \mathbf{0.919} \cdot \boldsymbol{e}^{(-\boldsymbol{e}^{\mathbf{0.0000163} - \mathbf{0.285} \cdot \boldsymbol{Age}})}\right)$$ **Equation S13**

The median and 5$^{th}$ to 95$^{th}$ percentiles of the predicted $fm_{CYP3A}$ in infants aged 2 to 4 months old using these *in vivo* FMO3 ontogeny functions Models 2, 3 and 6 were almost identical (**Fig. S23-B**). The median of the predicted $fm_{CYP3A}$ was consistently below 20%, indicating a comparable or even lower propensity to CYP3A victim DDI as in older children and adults. Similarly, the predicted midazolam AUC and $C_{max}$ ratios were also consistent among the *in vivo* FMO3 ontogeny function Models 2, 3 and 6 (**Fig. S23-C and D**). The predicted geometric mean of ratios were <1.25 across the age range and 95$^{th}$ percentiles of the predictions were well below 2-fold. Therefore, the impact of the variable FMO3 predictions on the CYP3A-mediated DDI predictions for risdiplam in infants aged 2 to 4 months old is considered negligible.

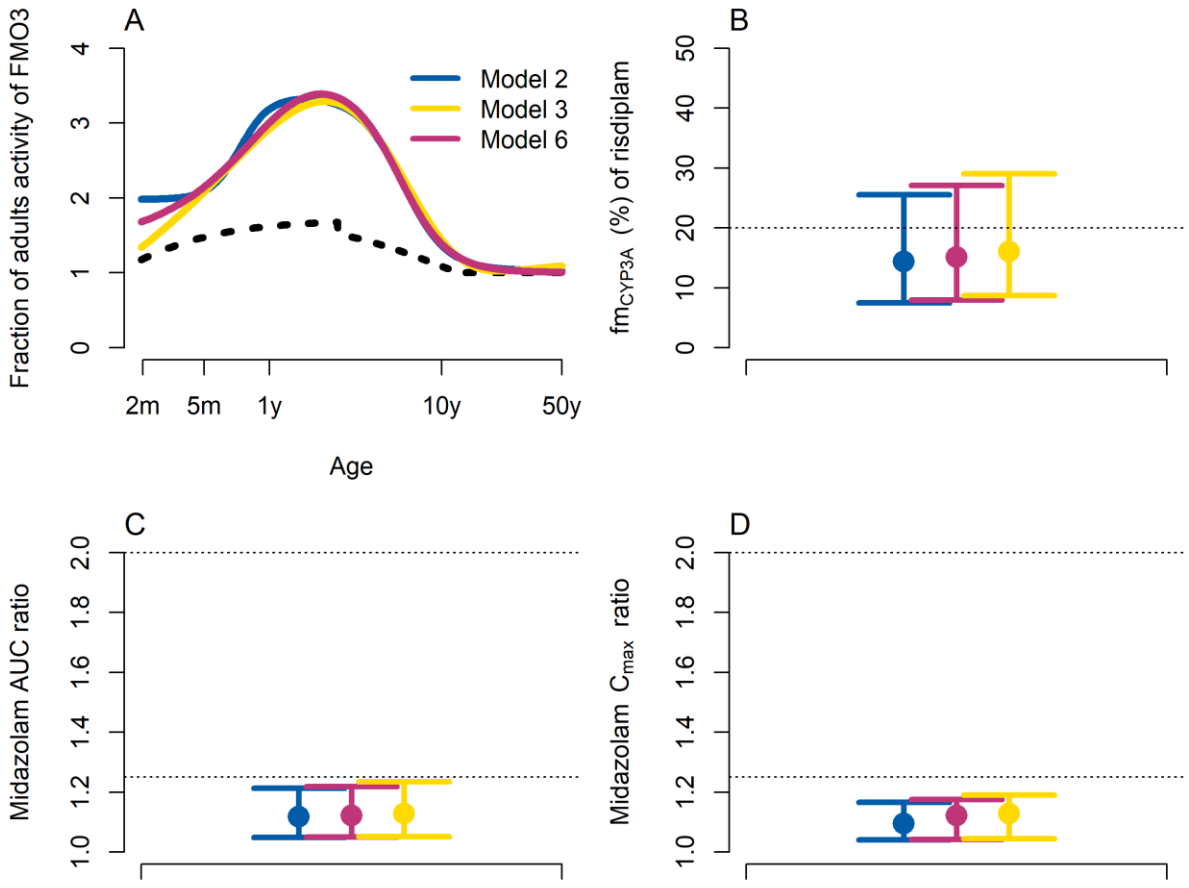


**Fig. S23 CYP3A-mediated DDI prediction for risdiplam in infants aged 2 to 4 months old using the three estimated *in vivo* FMO3 ontogeny functions (Models 2, 3 and 6)**

(**A**) The estimated *in vivo* FMO3 ontogeny function Models 2, 3 and 6 are shown with the Upreti function for the hepatic CYP3A ontogeny (dotted lines) as a reference. (**B**) The predicted risdiplam $fm_{CYP3A}$ in infants aged 2 to 4 months old using the *in vivo* FMO3 ontogeny function Models 2, 3 and 6. The circles and the whiskers indicate the median and 5$^{th}$ to 95$^{th}$ percentiles of the predictions, respectively and the color corresponds to the respective ontogeny shown in (**A**). (**C**) and (**D**) show predicted fold-increase in midazolam AUC and $C_{max}$ ratios in infants aged 2 to 4 months old by concomitant administration of risdiplam. The circles and the whiskers indicate the geometric mean and 5$^{th}$ to 95$^{th}$ percentiles of the predictions, respectively and the color corresponds to the respective ontogeny shown in (**A**). For the TDI simulations, Upreti and Johnson functions for the hepatic and intestinal CYP3A ontogeny functions, respectively and risdiplam *in vivo* TDI parameters, i.e., 18-fold lower *in vitro* TDI parameters were used.

### 9.3.2 Dual CYP3A-FMO3 substrates

The impact of the variable FMO3 ontogenies on the CYP3A-victim DDI predictions was also examined for the theoretical dual CYP3A-FMO3 substrates in infants aged 2 to 4 months old. The estimated *in vivo* FMO3 ontogeny functions Models 2, 3 and 6 (**Fig. S24**-A) were used for predictions of $fm_{CYP3A}$ and the ratios of AUCR between children and adults of Substrates A-C in infants aged 2 to 4 months old (**Fig. S24**-B and C). The predicted $fm_{CYP3A}$ were all lower than the corresponding values of adults and the difference was larger as the predicted FMO3 activity increased (i.e. Model 2 > Model 6 > Model 3). Consistently with the predictions for the population ≥4 months old (Figure 4), lower CYP3A-AUCRs than adults were shown in this age range, and the extent of difference increased with $fm_{CYP3A}$. Variable ranges of CYP3A-AUCR were predicted among the FMO3 ontogeny functions and the range was wider for Substrate C with $fm_{CYP3A}$=90%, than the others, reflecting high sensitivity to changes in $fm_{CYP3A}$ in the DDI prediction. In all cases, the predicted CYP3A-AUCR of these infants remained comparable or lower than adults even with the most conservative FMO3 ontogeny function Model 3, since all FMO3 models predict comparable or higher FMO3 activity than that of CYP3A by Upreti function in the age range ≥2 months old.

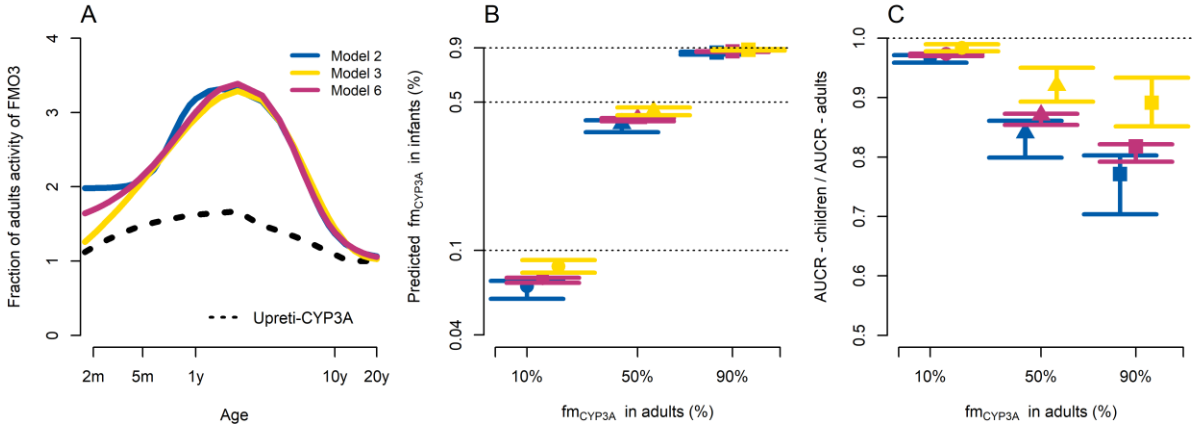


**Fig. S24 CYP3A DDI risk assessments for theoretical dual CYP3A and FMO3 substrates in infants aged 2 to 4 months old using the estimated *in vivo* FMO3 ontogeny functions Models 2, 3 or 6.**

(**A**) The estimated *in vivo* FMO3 ontogeny function Models 2, 3 and 6 are shown with the Upreti function for the hepatic CYP3A ontogeny (dotted lines) as a reference. (**B**) The median and range of predicted $fm_{CYP3A}$ in infants aged 2 to 4 months old compared to the parameter values in adults and (**C**) The median and range of the predicted AUCR ratios in infants aged 2 to 4 months old and adults for the theoretical dual CYP3A-FMO3 substrates. The $fm_{CYP3A}$:$fm_{FMO3}$ of 0.1:0.9 (Substrate A-circle), 0.5:0.5 (Substrate B- triangles) and 0.9:0.1 (Substrate C- squares) are values in adults. The symbols and whiskers represent the median and range of the predictions, respectively and the color corresponds to the respective FMO3 ontogeny shown in (**A**).

## 10. Allometric scaling of CL/F in the PPK model of risdiplam

Body weight, liver weight and allometric scaling factor of the risdiplam database were compared in **Fig. S25**. The liver weight was calculated according to Equation S3, allometric scaling factor was calculated with a reference body weight of 70 kg and an exponent of 0.75 [22]. The relationships to body weight were similar between the liver weight (left) and the allometric scaling factor (middle), and there is correlation between the liver weight and the allometric scaling factor. Consistent relationships were shown when body composition [23] was considered in the allometric scaling factor.

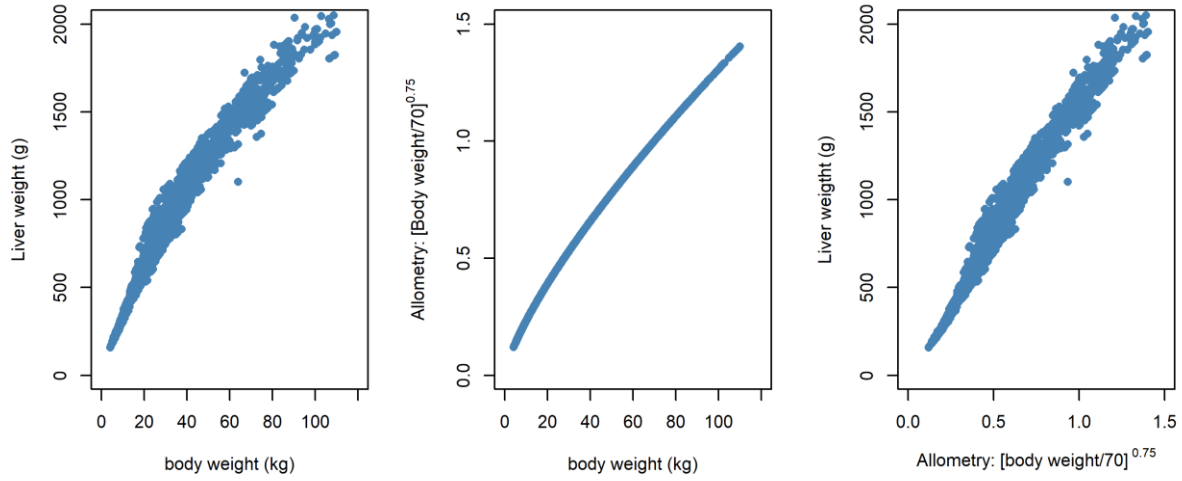


**Fig. S25 Relationship among body weight, liver weight and allometric scaling factor.**

A PPK model of risdiplam with allometric exponent of 0.75 on CL/F and 1.0 on volume of distributions without maturation function was fitted to the data (n=525, 2 months to 61 years old). The distribution of ETA-CL/F over the age range is biased. Compared to adults, the CL/F is higher in children 6 months to 10 years old which is in agreement with the estimated *in vivo* FMO3 ontogeny by the Mech-PPK modelling.

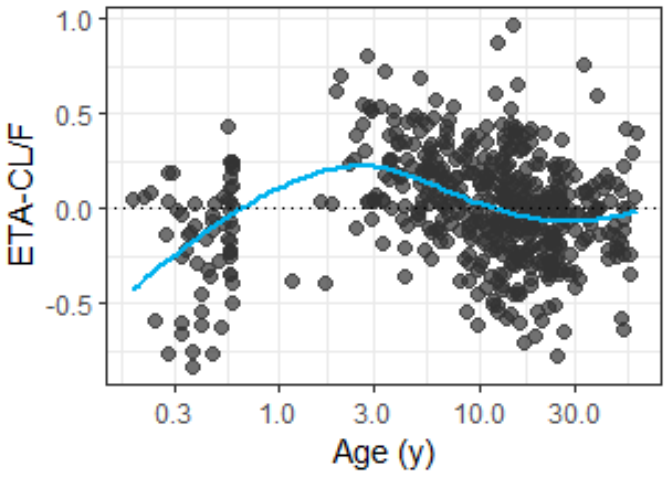


**Fig. S26 Distribution of ETA-CL/F of the PPK model with the theory-based allometric exponent 0.75 over the age range.**

Blue line indicates smooth

## 11. Impact of uncertainty in CYP3A ontogeny on the estimation of *in vivo* FMO3 ontogeny

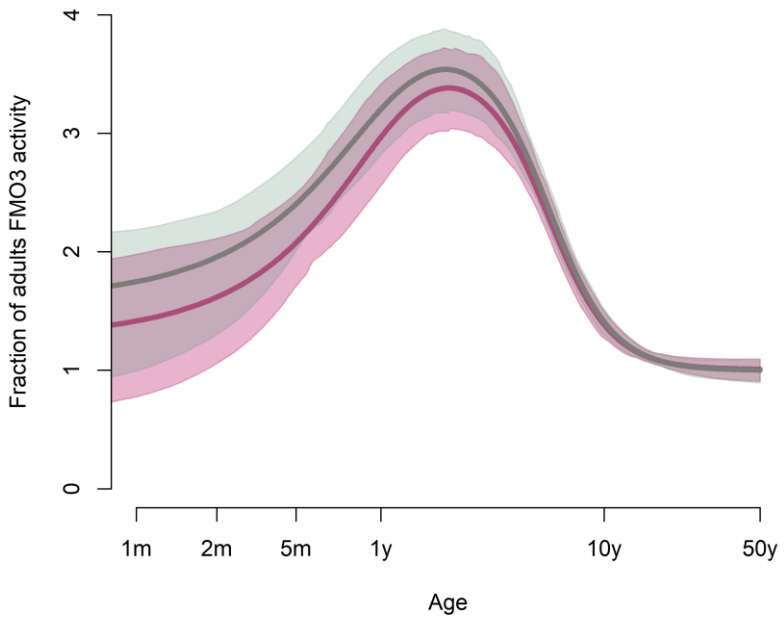


**Fig. S27 *in vivo* FMO3 ontogeny Model 6 estimated by the mechanistic PPK model of risdiplam with Upreti or Salem ontogeny functions for CYP3A ontogeny and 95% confidence intervals.**

Predictions of *in vivo* FMO3 ontogeny by Model 6 using Upreti (magenta) or Salem (green) functions for CYP3A ontogeny and their respective 95% confidence intervals ($2.5^{th}$ to $97.5^{th}$ percentiles of predicted fraction of adults FMO3 activity by bootstrap analyses with 200 estimates) between 2 months and 50 years old are shown with a solid line and shaded area, respectively.

## 12. References


1. Sturm, S., et al., *A phase 1 healthy male volunteer single escalating dose study of the pharmacokinetics and pharmacodynamics of risdiplam (RG7916, RO7034067), a SMN2 splicing modifier.* Br J Clin Pharmacol, 2019. **85**(1): p. 181-193.
2. Cleary, Y., et al., *Model-Based Drug-Drug Interaction Extrapolation Strategy From Adults to Children: Risdiplam in Pediatric Patients With Spinal Muscular Atrophy.* Clin Pharmacol Ther, 2021. **110**(6): p. 1547-1557.
3. Agency, E.M., *Assessment report Evrysdi.* https://www.ema.europa.eu/en/documents/assessment-report/evrysdi-epar-public-assessment-report_en.pdf Accessed May 2022, 2021.
4. Mercuri, E., et al., *Safety and efficacy of once-daily risdiplam in type 2 and non-ambulant type 3 spinal muscular atrophy (SUNFISH part 2): a phase 3, double-blind, randomised, placebo-controlled trial.* Lancet Neurol, 2022. **21**(1): p. 42-52.
5. Baranello, G., et al., *Risdiplam in Type 1 Spinal Muscular Atrophy.* N Engl J Med, 2021. **384**(10): p. 915-923.
6. Darras, B.T., et al., *Risdiplam-Treated Infants with Type 1 Spinal Muscular Atrophy versus Historical Controls.* N Engl J Med, 2021. **385**(5): p. 427-435.
7. Fowler, S., et al., *Addressing Today's Absorption, Distribution, Metabolism, and Excretion (ADME) Challenges in the Translation of In Vitro ADME Characteristics to Humans: A Case Study of the SMN2 mRNA Splicing Modifier Risdiplam.* Drug Metab Dispos, 2022. **50**(1): p. 65-75.

8. Upreti, V.V. and J.L. Wahlstrom, *Meta-analysis of hepatic cytochrome P450 ontogeny to underwrite the prediction of pediatric pharmacokinetics using physiologically based pharmacokinetic modeling.* J Clin Pharmacol, 2016. **56**(3): p. 266-83.
9. Salem, F., et al., *A re-evaluation and validation of ontogeny functions for cytochrome P450 1A2 and 3A4 based on in vivo data.* Clin Pharmacokinet, 2014. **53**(7): p. 625-36.
10. Xu, M., et al., *Genetic and Nongenetic Factors Associated with Protein Abundance of Flavin-Containing Monooxygenase 3 in Human Liver.* J Pharmacol Exp Ther, 2017. **363**(2): p. 265-274.
11. Koukouritaki, S.B., et al., *Human hepatic flavin-containing monooxygenases 1 (FMO1) and 3 (FMO3) developmental expression.* Pediatr Res, 2002. **51**(2): p. 236-43.
12. Shimizu, M., et al., *Developmental variations in metabolic capacity of flavin-containing mono-oxygenase 3 in childhood.* Br J Clin Pharmacol, 2011. **71**(4): p. 585-91.
13. DuBois D, D.E., *A formula to estimate the approximate surface area if height and weight are known.* Arch Intern Med, 1916. **17**: p. 863-871.
14. Haycock, G.B., G.J. Schwartz, and D.H. Wisotsky, *Geometric method for measuring body surface area: a height-weight formula validated in infants, children, and adults.* J Pediatr, 1978. **93**(1): p. 62-6.
15. Johnson, T.N., A. Rostami-Hodjegan, and G.T. Tucker, *Prediction of the clearance of eleven drugs and associated variability in neonates, infants and children.* Clin Pharmacokinet, 2006. **45**(9): p. 931-56.
16. Barter, Z.E., et al., *Covariation of human microsomal protein per gram of liver with age: absence of influence of operator and sample storage may justify interlaboratory data pooling.* Drug Metab Dispos, 2008. **36**(12): p. 2405-9.
17. Leeder, J.S., et al., *Ontogeny of Scaling Factors for Pediatric Physiology-Based Pharmacokinetic Modeling and Simulation: Microsomal Protein Per Gram of Liver.* Drug Metab Dispos, 2022. **50**(1): p. 24-32.
18. Guyton AC, H.J., *Cardiac output, venous return, and their regulation. In: Guyton AC, Hall JE, editors.* Textbook of medical physiology. 9th ed. Philadelphia (PA): WB Saunders, 1996: p. 1148.
19. *Basic anatomical and physiological data for use in radiological protection: reference values. A report of age- and gender-related differences in the anatomical and physiological characteristics of reference individuals. ICRP Publication 89.* Ann ICRP, 2002. **32**(3-4): p. 5-265.
20. FDA, U., *Center for Drug Evaluation and Reserach. Application Number: 213535Orig1s000 Clinical Pharmacology Review(s).* https://www.accessdata.fda.gov/drugsatfda_docs/nda/2020/213535Orig1s000ClinPharmR.pdf, 2020. **Accessed May 2022.**
21. FDA, U., *EVRYSDI™ (risdiplam) for oral solution. Highlights of Prescribing Information.* https://www.accessdata.fda.gov/drugsatfda_docs/nda/2020/213535Orig1s000lbl.pdf, 2020. **Accessed March 2022.**
22. Anderson, B.J. and N.H. Holford, *Mechanism-based concepts of size and maturity in pharmacokinetics.* Annu Rev Pharmacol Toxicol, 2008. **48**: p. 303-32.
23. Gonzalez-Sales, M., et al., *Wide size dispersion and use of body composition and maturation improves the reliability of allometric exponent estimates.* J Pharmacokinet Pharmacodyn, 2022. **49**(2): p. 151-165.